Applications of the synchrosqueezing transform in seismic time-frequency analysis

Roberto H. Herrera[1], Jiajun Han[1], and Mirko van der Baan[1]

ABSTRACT

Time-frequency representation of seismic signals provides a source of information that is usually hidden in the Fourier spectrum. The short-time Fourier transform and the wavelet transform are the principal approaches to simultaneously decompose a signal into time and frequency components. Known limitations, such as trade-offs between time and frequency resolution, may be overcome by alternative techniques that extract instantaneous modal components. Empirical mode decomposition aims to decompose a signal into components that are well separated in the time-frequency plane allowing the reconstruction of these components. On the other hand, a recently proposed method called the "synchrosqueezing transform" (SST) is an extension of the wavelet transform incorporating elements of empirical mode decomposition and frequency reassignment techniques. This new tool produces a well-defined time-frequency representation allowing the identification of instantaneous frequencies in seismic signals to highlight individual components. We introduce the SST with applications for seismic signals and produced promising results on synthetic and field data examples.

INTRODUCTION

This paper is a follow-up study of the empirical mode decomposition (EMD) method (Han and Van der Baan, 2013). The EMD method is an effective way to decompose a seismic signal into individual components, called "intrinsic mode functions" (IMFs). Each IMF represents a harmonic signal localized in time, with slowly varying amplitudes and frequencies, potentially highlighting different geologic and stratigraphic information.

EMD methods have evolved from EMD to ensemble EMD (Wu and Huang, 2009) and recently to complete ensemble EMD (CEEMD) (Torres et al., 2011). These extensions aim to solve the mode mixing problem (Huang et al., 1999, 2003) while keeping the complete reconstruction capability. Han and Van der Baan (2013) investigate the difference between these EMD methods, and discuss the suitability of EMD for seismic interpretation. They conclude that CEEMD not only solves the mode mixing problem but also provides an exact reconstruction of the original signal. In terms of spectral resolution, the EMD-based alternatives outperform the short-time Fourier transform (STFT) and the wavelet transform (WT) methods. Yet, like other methods, the top-performing CEEMD still has limitations when the components are not well separated in the time-frequency plane.

We extend our studies of time-frequency analysis with a recently proposed transform called the "synchrosqueezing transform" (SST) (Daubechies et al., 2011). SST is a wavelet-based time-frequency representation that resembles the EMD method. Unlike EMD, it has a firm theoretical foundation (Wu et al., 2011; Thakur et al., 2013). SST is also an adaptive and invertible transform that improves the readability of a wavelet-based time-frequency map using frequency reassignment (Auger and Flandrin, 1995), by condensing the spectrum along the frequency axis (Li and Liang, 2012). This transform was originally proposed in the field of audio processing (Daubechies et al., 2011) and has been successfully applied to paleoclimate time series (Thakur et al., 2013) and to vibration monitoring (Li and Liang, 2012). The SST is still limited by Gabor's uncertainty principle (Hall, 2006), but it approximates the lower limit better, thus improving resolution.

In this paper, we show the suitability of SST in seismic time-frequency representation. We contrast and compare SST with CEEMD and the continuous wavelet transform (CWT). Our selection of CEEMD as a reference method for comparison is based on its very low reconstruction errors (Torres et al., 2011) and the fact that it was successfully applied to seismic signal analysis (Han and Van der Baan, 2013), where the instantaneous frequencies are

estimated as a posterior step. The CWT is also taken as a reference because SST comprises a combination of this method with frequency reassignment.

In the following section, we describe the theory behind EMD and the SST. Next, we test the SST on a synthetic example and compare its time-frequency representation and signal reconstruction features with the CWT and CEEMD method. Finally, we apply SST on field data showing its potential to highlight stratigraphic features with high precision.

THEORY

A brief recap of EMD and siblings

EMD is a fully data-driven method to split a signal into components, called IMFs (Huang et al., 1998). Recursive empirical operations (sifting process; see Huang et al., 1998) separate the signal into high and low oscillatory components. The sum of all the individual components reproduces the original signal. However, some mode mixing appears in the classic EMD method, caused by signal intermittency (Huang et al., 1999, 2003), that can produce difficulties in interpreting the resulting time-frequency distribution. This fact triggered the development of ensemble EMD (Wu and Huang, 2009), which is based on a noise-injection technique. Noise is added prior to decomposition, and ensemble averages are computed for resulting IMFs. This aids in better separation of independent modes but does not guarantee perfect reconstruction.

Despite the improvement in mode separation using the noise-assisted technique, reconstruction from individual components is important, and Torres et al. (2011) propose an elegant solution. In the CEEMD, an appropriate noise signal is added at each stage of the decomposition producing a unique signal residual for computing the next IMF (Torres et al., 2011; Han and Van der Baan, 2013). Computation of the instantaneous frequencies for each IMF then produces the desired time-frequency representation (Han and Van der Baan, 2013).

The synchrosqueezing transform

The SST was originally introduced in the context of audio signal analysis and is shown to be an alternative to EMD (Daubechies and Maes, 1996; Daubechies et al., 2011). SST aims to decompose a signal $s(t)$ into constituent components with time-varying harmonic behavior. These signals are assumed to be the addition of individual time-varying harmonic components yielding

$$s(t) = \sum_{k=1}^{K} A_k(t) \cos(\theta_k(t)) + \eta(t), \quad (1)$$

where $A_k(t)$ is the instantaneous amplitude, $\eta(t)$ represents additive noise, K stands for the maximum number of components in one signal, and $\theta_k(t)$ is the instantaneous phase of the k_{th} component. The instantaneous frequency $f_k(t)$ of the k_{th} component is estimated from the instantaneous phase as

$$f_k(t) = \frac{1}{2\pi} \frac{d}{dt} \theta_k(t). \quad (2)$$

In seismic signals, the number K of harmonics or components in the signal is infinite. They can appear at different time slots, with different amplitudes $A_k(t)$, instantaneous frequencies $f_k(t)$, and they may be separated by their spectral bandwidths $\Delta f_k(t)$.

The spectral bandwidth defines the spreading around the central frequency, which in our case is the instantaneous frequency; see Barnes (1993) for a completed disentangling of concepts. This magnitude is a constraint for traditional time frequency representation methods. The STFT and the CWT tend to smear the energy of the superimposed instantaneous frequencies around their center frequencies (Daubechies and Maes, 1996). The smearing equals the standard deviation around the central frequency, which is the spectral bandwidth (Barnes, 1993).

SST is able to decompose signals into constituent components with time-varying oscillatory characteristics (Thakur et al., 2013). Thus, by using SST we can recover the amplitude $A_k(t)$ and the instantaneous frequency $f_k(t)$ for each component.

From CWT to SST

The CWT of a signal $s(t)$ is (Daubechies, 1992)

$$W_s(a, b) = \frac{1}{\sqrt{a}} \int s(t) \psi^* \left(\frac{t-b}{a}\right) dt, \quad (3)$$

where ψ^* is the complex conjugate of the mother wavelet and b is the time shift applied to the mother wavelet, which is also scaled by a. The CWT is the crosscorrelation of the signal $s(t)$ with several wavelets that are scaled and translated versions of the original mother wavelet. The symbols $W_s(a, b)$ are the coefficients representing a concentrated time-frequency picture, which is used to extract the instantaneous frequencies (Daubechies et al., 2011).

Daubechies et al. (2011) observe that there is a limit to reduce the smearing effect in the time-frequency representation using the CWT. Equation 3 can be rewritten using Plancherel's theorem, energy in the time domain equals energy in the frequency domain, i.e., Parseval's theorem in the Fourier domain:

$$W_s(a, b) = \frac{1}{2\pi} \int \frac{1}{\sqrt{a}} \hat{s}(\xi) \hat{\psi}^*(a\xi) e^{jb\xi} d\xi, \quad (4)$$

where $j = \sqrt{-1}$, ξ is the angular frequency, and $\hat{\psi}(\xi)$ is the Fourier transform of $\psi(t)$. The scale factor a modifies the frequency of the complex wavelet $\hat{\psi}^*(a\xi)$, by stretching and squeezing it. Also, the time shift b is represented by its Fourier pair $e^{jb\xi}$. The convolution in equation 3 becomes multiplication in the frequency domain in equation 4. Considering the simple case of a single harmonic signal $s(t) = A \cos(\omega t)$ with Fourier pair $\hat{s}(\xi) = \pi A[\delta(\xi - \omega) + \delta(\xi + \omega)]$, equation 4 can then be transformed into

$$W_s(a, b) = \frac{A}{2} \int \frac{1}{\sqrt{a}} [\delta(\xi - \omega) + \delta(\xi + \omega)] \hat{\psi}^*(a\xi) e^{jb\xi} d\xi,$$

$$= \frac{A}{2\sqrt{a}} \hat{\psi}^*(a\omega) e^{jb\omega}. \quad (5)$$

In the frequency plane, if the wavelet $\hat{\psi}^*(\xi)$ is concentrated around its central frequency $\xi = \omega_0$, then $W_s(a, b)$ will be concentrated around the scale $a = \omega_0/\omega$ (the ratio of the central frequency of the wavelet to the central frequency of the signal). However, what we actually get is that $W_s(a, b)$ often spreads out along the scale axis leading to a blurred projection in time-scale representation.

This smearing mainly occurs in the scale dimension a, for constant time offset b (Li and Liang, 2012). Daubechies and Maes (1996) show that if smearing along the time axis can be neglected, then the instantaneous frequency $\omega_s(a, b)$ can be computed as the derivative of the WT at any point (a, b) with respect to b, for all $W_s(a, b) \neq 0$:

$$\omega_s(a, b) = \frac{-j}{2\pi W_s(a, b)} \frac{\partial W_s(a, b)}{\partial b}. \qquad (6)$$

The final step in the new time-frequency representation is to map the information from the time-scale plane to the time-frequency plane. Every point (b, a) is converted to $(b, \omega_s(a, b))$, and this operation is called synchrosqueezing (Daubechies et al., 2011). Because a and b are discrete values, we can have a scaling step $\Delta a_k = a_{k-1} - a_k$ for any a_k where $W_s(a, b)$ is computed. Likewise, when mapping from the time-scale plane to the time-frequency plane $(b, a) \rightarrow (b, w_{inst}(a, b))$, the SST $T_s(w, b)$ is determined only at the centers ω_l of the frequency range $[\omega_l - \Delta\omega/2, \omega_l + \Delta\omega/2]$, with $\Delta\omega = \omega_l - \omega_{l-1}$:

$$T_s(\omega_l, b) = \frac{1}{\Delta\omega} \sum_{a_k : |\omega(a_k, b) - \omega_l| \leq \Delta\omega/2} W_s(a_k, b) a^{-3/2} \Delta a_k. \quad (7)$$

The above equation shows that the new time-frequency representation of the signal $T_s(\omega_l, b)$ is synchrosqueezed along the frequency (or scale) axis only (Li and Liang, 2012). The SST reallocates the coefficients of the CWT to get a concentrated image over the time-frequency plane, from which the instantaneous frequencies are then extracted (Wu et al., 2011).

Following Thakur et al. (2013), the discretized version of $T_s(\omega_l, b)$ in equation 7 is represented by $\tilde{T}_{\tilde{s}}(w_l, t_m)$, where t_m is the discrete time $t_m = t_0 + m\Delta t$ with Δt the sampling rate and $m = 0, \ldots, n-1$; n is total number of samples in the discrete signal $\tilde{s}_m$. More special considerations are described in Thakur et al. (2013). The reconstruction of the individual components s_k from the discrete synchrosqueezed transform $\tilde{T}_{\tilde{s}}$ is then the inverse CWT over a small frequency band $l\epsilon L_k(t_m)$ around the kth component:

$$s_k(t_m) = 2C_\phi^{-1} \Re e \left(\sum_{l\epsilon L_k(t_m)} \tilde{T}_{\tilde{s}}(w_l, t_m) \right), \qquad (8)$$

where C_ϕ is a constant dependent on the selected wavelet. As we take the real part $\Re e$ of the discrete SST in that band, we recover the real component s_k. In this paper, we follow Thakur et al. (2013) in which the reconstruction is done by a standard least-squares ridge extraction method; different approaches are explored by Meignen et al. (2012).

Parameter selection

The wavelet choice is a key issue in synchrosqueezing-based methods (Meignen et al., 2012). In SST, we first construct the time-frequency map through a CWT; thus, we need a mother wavelet that satisfies the admissibility condition (i.e., finite energy, zero mean, and bandlimited). At the same time, the wavelet must be a good match for the target signal (Mallat, 2008). By definition, the wavelet coefficients are the correlation coefficients between the target signal and dilated and translated versions of a given basic pattern

(Daubechies, 1992). In our implementation, we use a Morlet wavelet with central frequency and bandwidth estimated from the seismic signal.

The other parameter of interest is the wavelet threshold γ. It effectively decides the lowest usable magnitude in the CWT (Thakur et al., 2013). It is a noise-based hard thresholding that Thakur et al. (2013) set to 10^{-8} for the ideal noiseless case in double precision machines. In real cases, when the noise level is unknown, it is common practice to use the finest scale of the wavelet decomposition (Donoho, 1995) as the noise variance σ_η^2. This threshold works in real signals as a noise-level adaptive estimator (Herrera et al., 2006) and is defined as the median absolute deviation (MAD) of the first octave (Donoho, 1995; Thakur et al., 2013):

$$\sigma_\eta = \text{median}(|W_s(a_{1:n_v}, b) \\ - \text{median}(W_s(a_{1:n_v}, b))|)/0.6745, \qquad (9)$$

where $W_s(a_{1:n_v}, b)$ are the finest scale wavelet coefficients and 0.6745 is a normalizing factor being the MAD of a Gaussian distribution. The threshold is then weighted by the signal length n to be asymptotically optimal with value $\gamma = \sqrt{2 \log n} \cdot \sigma_\eta$.

EXAMPLES

Synthetic data

In this section, we test the SST with a challenging synthetic signal (Figure 1). This is the same synthetic example used by Han and Van der Baan (2013). The signal is comprised of an initial 20 Hz cosine wave, with a 100 Hz Morlet atom at 0.3 s, two 30 Hz zero-phase Ricker wavelets at 1.07 and 1.1 s, and three different frequency components between 1.3 and 1.7 s of, respectively, 7, 30, and 40 Hz. Note that the 7 Hz frequency component is split into three parts less than a full period each, appearing at 1.37, 1.51, and 1.65 s.

Figure 2a shows the CWT, CEEMD, and SST time-frequency representations. For comparison purposes, we include the CWT result, because the SST is an extension of the CWT. The STFT is known to have suboptimal performance, as is shown in Figure 6
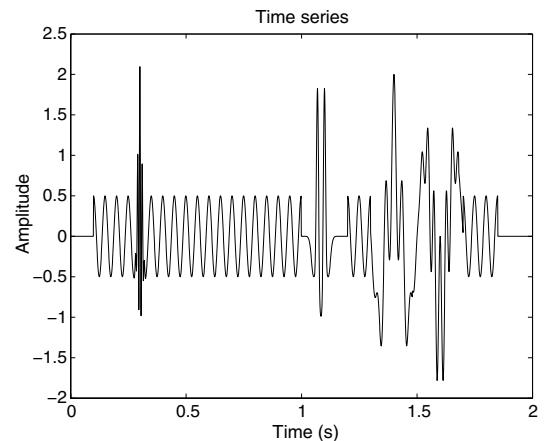

Figure 1. Synthetic example: background 20 Hz cosine wave, superposed 100 Hz Morlet atom at 0.3 s, two 30 Hz Ricker wavelets at 1.07 and 1.1 s, and there are three different frequency components between 1.3 and 1.7 s. Same as Figure 1 in Han and Van der Baan (2013).
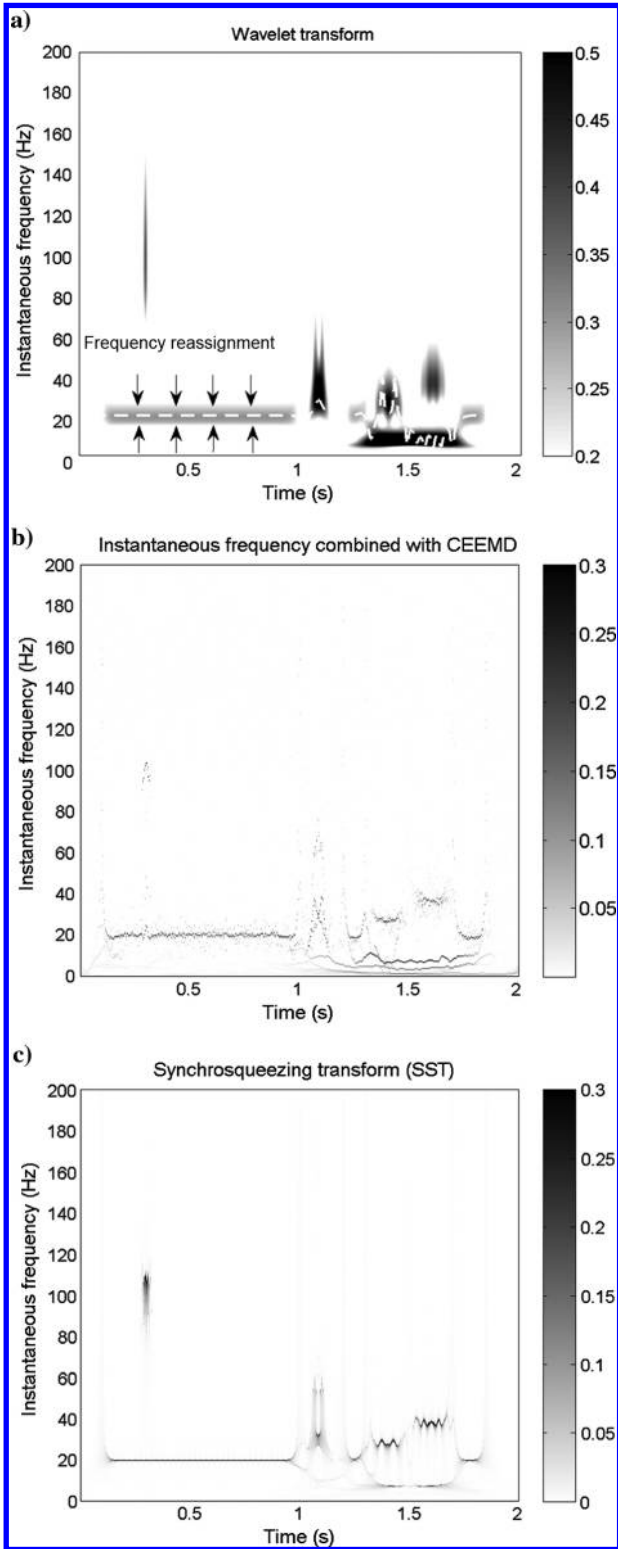
Figure 2. Time-frequency representation of the synthetic trace. (a) CWT, displaying smearing along the frequency axis for the harmonic signals with a sketch of the SST procedure. (b) CEEMD output with 10% added Gaussian white noise and 100 realizations. The instantaneous frequencies corresponding to individual components are well delineated. (c) SST output, with similar results for the harmonics as CEEMD.

of Han and Van der Baan (2013). In Han and Van der Baan (2013), a 2D Gaussian smoothing filter (7×7 samples) was applied to the CEEMD and SST outputs to improve visualization. In our examples, we plot the actual outputs from each method, because the objective is to show the sharpness of the reconstructed instantaneous frequencies.

CWT uses a Morlet mother wavelet and a total of 320 scales (32 voices per octave) to provide the time-frequency map shown in Figure 2a. Note that this is the same result as in Figure 7 of Han and Van der Baan (2013) with a different color scale. Here, we have added a graphical interpretation to illustrate how the synchrosqueezed representation is derived from the CWT. The dashed white line in the vicinity of 20 Hz in Figure 2a is the ridge obtained from the instantaneous frequency in the wavelet domain from equation 6. The next step involves the reassignment of the CWT values to the position indicated by the instantaneous frequency ω_l in equation 7. This mapping process indicated by vertical arrows moves each point (b, a) to the location $(b, w_{\text{inst}}(a, b))$ producing a new time frequency representation that is shown in Figure 2c. CEEMD (Figure 2b) uses 10% of injected Gaussian white noise and 100 realizations. The result obtained by the SST (Figure 2c) uses, likewise, the CWT from which it was generated, a Morlet wavelet, and 32 voices per octave.

CEEMD and SST delineate the individual components equally well; especially, the instantaneous frequencies for the harmonic signals are well resolved. Yet, CEEMD collapses the short 100 Hz Morlet wavelet at 0.3 s more. The 7, 30, and 40 Hz frequency components occurring between 1.3 and 1.7 s are resolved by both methods, but there is little indication that the 7 Hz component is not continuous. SST and CEEMD show only minor differences, but both display significantly less frequency smearing than the CWT representation.

Unlike the CWT, SST and CEEMD allow for the extraction of the individual components. Here, we compare the performance of both methods in extracting and reconstructing the modes in a signal. To numerically evaluate the reconstruction error, for both decompositions, we use the difference between the original signal and the sum of the modes (Torres et al., 2011). A more general metric based on the mean square error (MSE) is used to score reconstruction with a single value as

$$\text{MSE} = \frac{1}{N} \sum_{n=0}^{N-1} |s(t) - \hat{s}(t)|^2, \tag{10}$$

where N is the number of samples, $s(t)$ is the original signal, and $\hat{s}(t)$ is the reconstructed signal from the sum of all modes.

Figure 3 shows the IMFs (IMFs) extracted with the CEEMD. The CEEMD decomposition is able to unmix each individual component giving an easily interpretable decomposition. On the other hand, the SST method (Figure 4) shows some degree of mode mixing of the components.

For the CEEMD method, the first IMF shows the 100 Hz Morlet atom, which is also identified by SST IMF1, but SST also recovers parts of the 30 Hz Ricker wavelets. IMF2 of both methods are the residuals of the high-frequency components. IMF3 of the CEEMD represents the higher oscillations in the upper band of the Ricker wavelets, whereas IMF3 of the SST shows directly the 30 Hz Ricker wavelets plus the 30 and 40 Hz component. For IMF4, the SST method performs equally as well as the CEEMD does, but it in-

cludes the 20 Hz component between the two 30 Hz. IMF5 of the CEEMD shows the 20 Hz component with some mixtures of the 30 Hz Ricker wavelets, whereas the SST shows a better representation of the 20 Hz with the 7 Hz mode. IMF6 is only informative for CEEMD with an isolated 7 Hz mode. The remainder are small-valued elements. These low-amplitude components in the CEEMD method are low-amplitude frequency bands, derived during the sifting process. IMFs are derived from the highest oscillating components to the lower frequency ones. Like the Fourier transform, some IMFs will have higher amplitudes than other components depending on the signal characteristics. This is visible in Figure 3, where the second IMF has not only a different frequency content from IMF 1 and 3, but also a different maximum amplitude.

The reconstructed signals by both methods are shown in Figure 5. CEEMD (top dotted gray) has a perfect reconstruction subjected only to machine precision with an overall MSE value of 5×10^{-33} and a negligible reconstruction error as is shown in the bottom plot. The SST method provides a good estimation (top continuous line), but some areas are not reconstructed accurately, especially in the amplitudes, as is shown in the bottom plot (continuous line). The MSE for the SST is 0.0013, which is in the range of what is considered good performance for a reconstruction method (Meignen et al., 2012).

Application to field seismic signals

Single trace

In this section, we apply the SST to a field data set and compare to the CWT and CEEMD methods. This is a data set from a sedimentary basin in Canada (Figure 6), also analyzed by Han and Van der Baan (2013) and Van der Baan et al. (2010). It contains a Cretaceous meandering channel at 0.42 s between common midpoints (CMPs) 75–105 and a second channel between CMPs 160–180 of this migrated 2D cross section. An erosional surface is located between CMPs 35–50 around 0.4 s. The data also contain evidence of migration artifacts (smiles) at the left edge between 0.1 and 0.6 s. There are bands of alternating high-frequency areas with tightly spaced reflections and low-frequency regions, which are mostly composed of blank intervals without much reflected energy (Van der Baan et al., 2010). This makes this data set interesting for testing time-frequency decomposition algorithms. It has been shown that both channel intersections exhibit significantly lower frequency content due to their increased thickness (Van der Baan
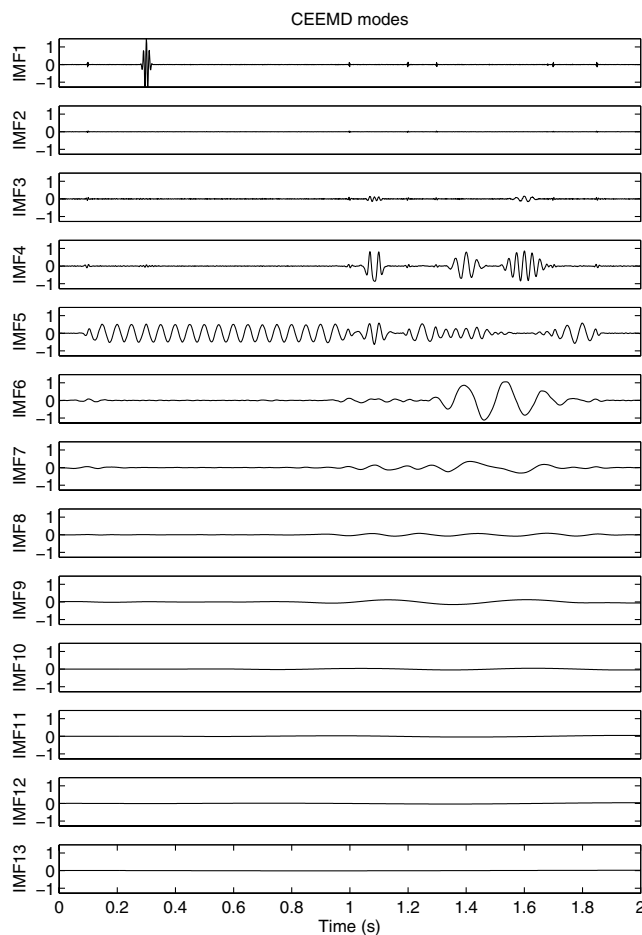

Figure 3. Decomposition of the original signal, shown in Figure 1, into its intrinsic modes by CEEMD. The decomposition gives 13 individual modes with little mode mixing.
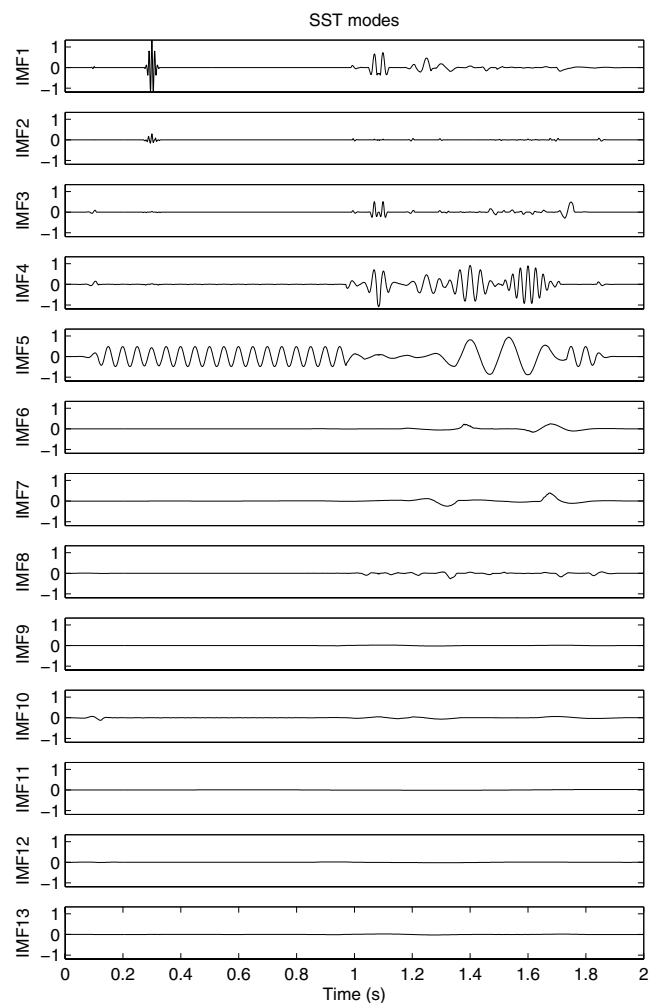

Figure 4. Decomposition of the original signal, shown in Figure 1, into its intrinsic modes by SST. We use the same 13 levels to compare to CEEMD output. Although the decomposition is able to isolate the individual components, still some degree of mode mixing is appreciable in the SST components.

et al., 2010), causing constructive interference in the low-frequency components (Partyka et al., 1999).

We take the seismic trace at CMP 81, which is plotted in Figure 7, and apply CWT, CEEMD, and SST as is shown in Figure 8. The CWT and SST methods are based on a Morlet wavelet with 32 voices per octave. CEEMD uses 10% of added Gaussian white noise and 50 realizations. Figure 12 in Han and Van der Baan (2013) shows the corresponding STFT plot.

All time-frequency representations display some similar shapes including the bright channel at 0.42 s and a decrease in frequency
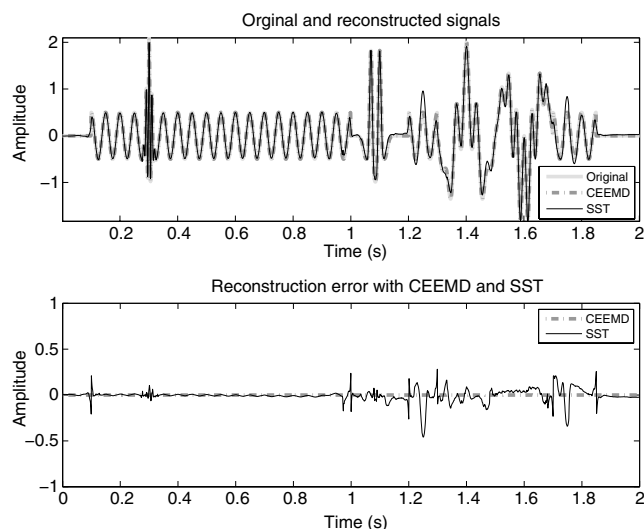
Figure 5. Reconstructed signals and reconstruction errors. (a) CEEMD estimate (gray dotted) over the original signal (continuous gray); there is no appreciable difference between these two signals. The reconstruction error is approximately zero, limited by the machine precision in the order of 10^{-16} (b). (b) SST produces a reasonable reconstruction (continuous line), especially for the stationary parts with an MSE value of 0.0013, which is a low reconstruction error.
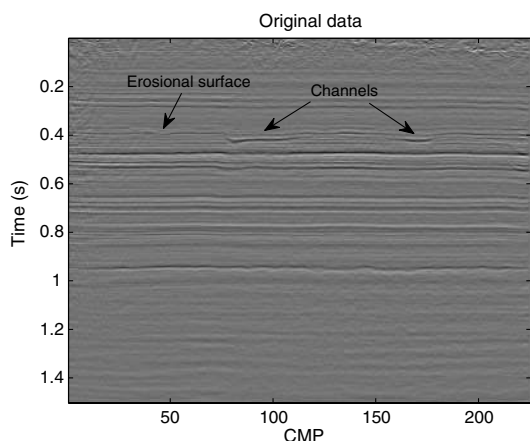

Figure 6. Seismic data set from a sedimentary basin in Canada. The erosional surface and channel sections are highlighted by arrows. The horizontal axis spans 5.6 km. Same data as in Figure 10 of Han and Van der Baan (2013).

content with time, most likely due to attenuation (Figure 8). The SST and CEEMD show more features than the CWT, due to the higher time-frequency resolution of both methods. SST and CEEMD representations generally agree for the frequencies above 50 Hz but connect strong spectral peaks differently for the lower frequencies. This demonstrates the value in examining a single time series using various time-frequency analysis methods.

Vertical cross section

Next, we apply the three methods to all traces and compute the frequency where the cumulative spectral energy is at 80% (C80) of the total energy (Perz, 2001; Van der Baan et al., 2010). Our motivation to use this cumulative energy criterion comes from the fact that frequency-dependent tuning effects are often analyzed using spectral decomposition to detect variations in turbidite layers or meandering channels (Partyka et al., 1999; Van der Baan et al., 2010). Low-frequency values in C80 indicate concentrations of energy near the lower portion of the total bandwidth, whereas high-frequency values imply a broader spectrum. In some cases, lower values will thus indicate areas of larger attenuation of the propagating wavelet. In other situations, it can reveal shifts in the position of a single notch in the locally observed wavelet, for instance, due to a thickening or thinning of reflector spacing (Van der Baan et al., 2010).

This frequency attribute is overlain onto the original seismic data shown in Figure 6. Figure 9 shows the CWT, CEEMD, and SST results. The color bar represents the frequency bands. This frequency representation for the three methods shows high- and low-frequency bands between 0.2 and 0.8 s due to variations in reflector spacing and a general decrease in high frequencies, which is associated with attenuation of the seismic wavelet.

The CWT C80 representation, shown in Figure 9a, brings out a broader picture of the spectral content of this spatial location; the major features are indicated. The CEEMD result emphasizes the most interesting features in the data set. Traces on the Cretaceous meandering channels at 0.42 s have lower frequency content than the neighboring traces. This low-frequency variation is due to the increased thickness in the channels. The SST result exhibits an even cleaner representation (Figure 9c). The thin layers around 0.8 s are
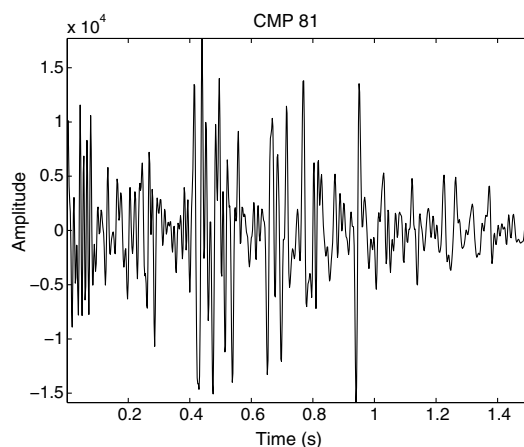

Figure 7. Individual trace at CMP 81 in Figure 6. It crosses the channel at 0.42 s.
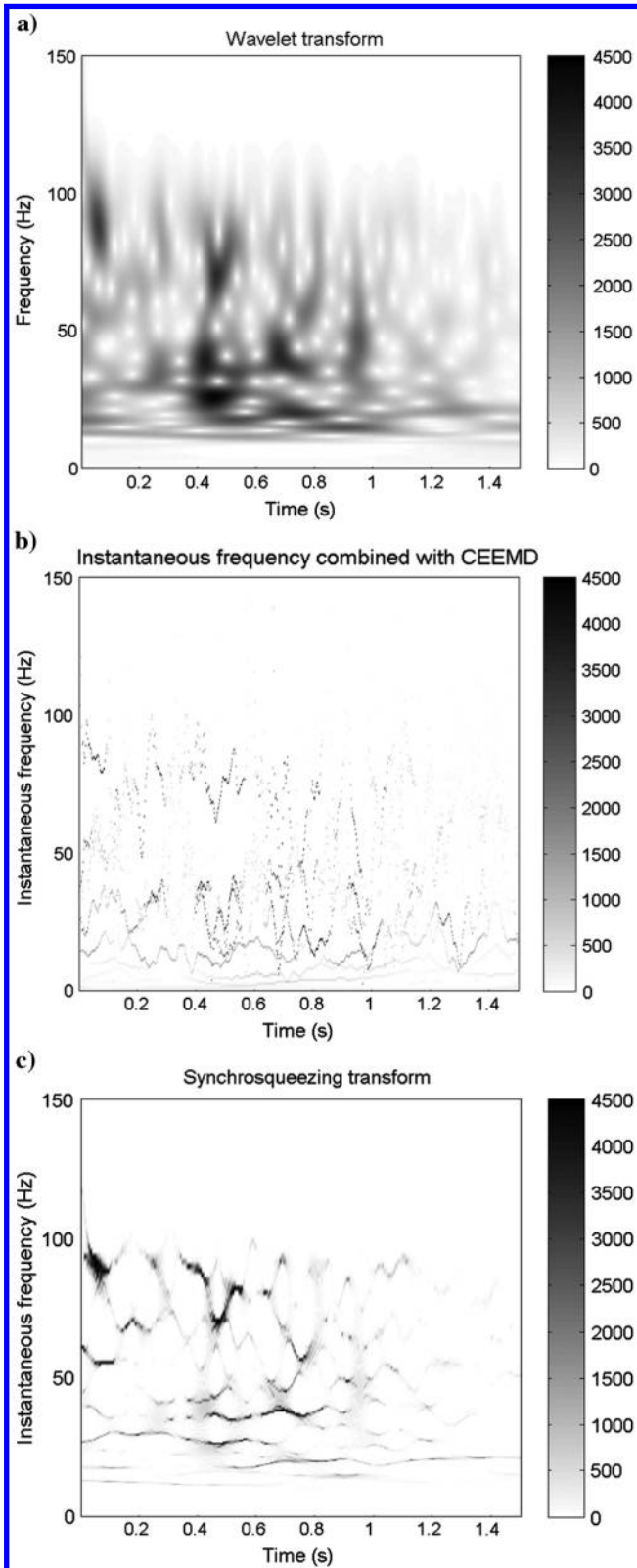
Figure 8. CMP 81. Time-frequency representation from (a) CWT, (b) CEEMD, and (c) SST. All show a decrease in frequency content over time, yet the CEEMD and SST results are least smeared.
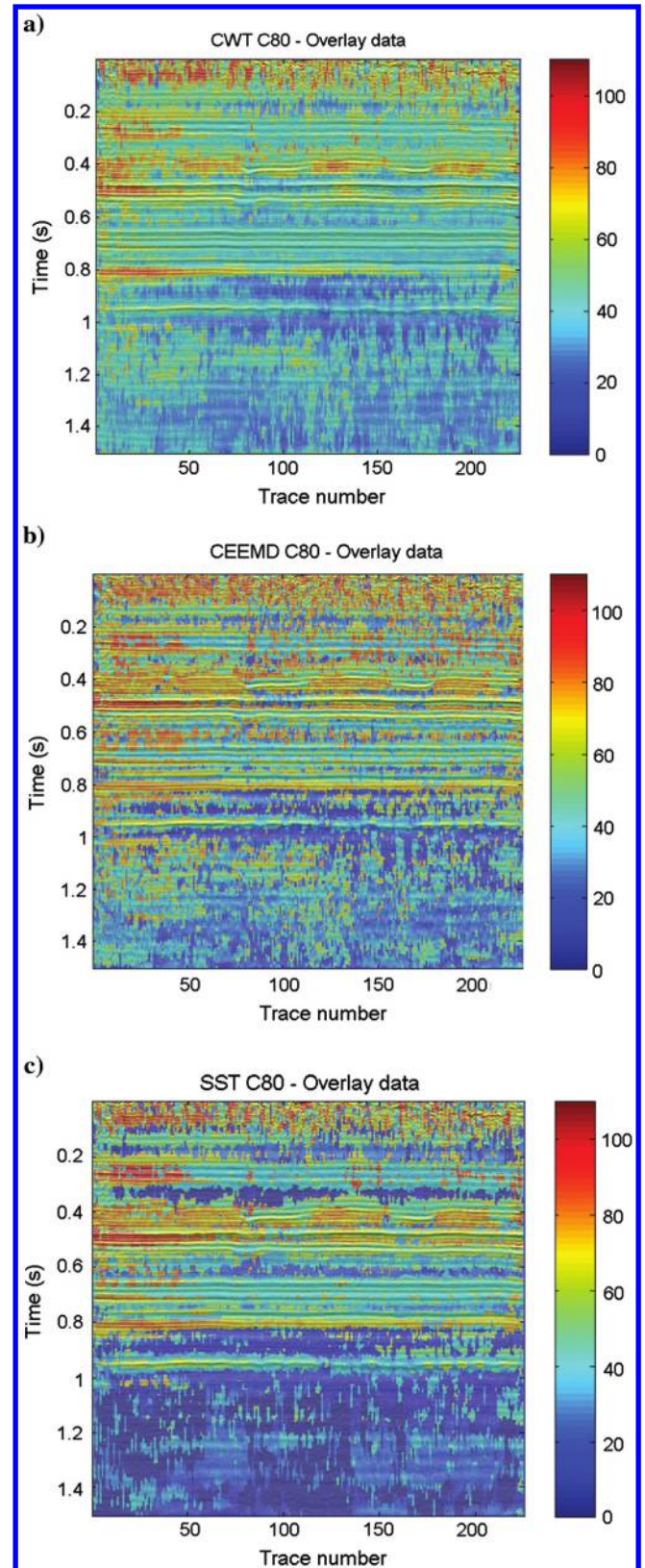

Figure 9. Characteristic frequencies for the vertical cross section. C80 attribute for (a) CWT, (b) CEEMD, and (c) SST. CEEMD and SST show a sparser representation than the CWT. SST has even less speckle noise, and the strong reflector at 0.9 s is better represented.

equally well identified by all methods, but fewer speckle like patterns are observed below this reflector in the CEEMD and SST images. The strong uniform reflector at 0.9 s is better represented by the SST method.

Horizontal slice

In our last test, we run the three algorithms on the entire seismic cube, composed of 225 inlines and 217 crosslines with a regular spacing of 25 m. Each trace is 450 samples long with a sampling period of 2 ms. Figure 10 shows the time slice at 420 ms of the seismic cube. Beside the channel, which is clearly shown throughout the image, there is a subtle fault. We compare the results of CWT, CEEMD, and SST centered at this time slice analyzing different frequency slices. CWT and SST use a Morlet wavelet with 32 levels per octave, and CEEMD injects 10% of Gaussian white noise using 50 realizations.

Figure 11 shows the resulting constant frequency slices for CWT (a), CEEMD (b), and SST (c) at, respectively, 20, 40, and 60 Hz (top to bottom). The channel and fault are more sharply represented by CEEMD and SST than in the CWT maps. CEEMD and SST have similar performance; however, only SST seems to show that the 60 Hz spectral component is fading.

The fault appears at the 40 and 60 Hz time slices of all three methods. The CWT shows the main features on all three frequency slices, yet their amplitude variations are less clear, which makes the thickness calculation of the channel challenging during further interpretation. Compared with CWT, the amplitude variation of CEEMD and SST along the channel is better defined, which is helpful to calculate subtle thickness variations. The amplitude variations between closely spaced frequencies are better resolved in the CEEMD and SST result due to significantly reduced frequency smearing and smaller spectral leakage than for the CWT and STFT methods (Han et al., 2013). In addition, the CWT depicts a rather homogeneous area in the zone to the right of the channel in all frequency slices, whereas the CEEMD and SST results show more

variable magnitudes with areas of localized amplitude strengthening and weakening plus several linear features.

DISCUSSION

SST can be used to accurately map time-domain signals into their time-frequency representation. It has a well-grounded mathematical foundation that facilitates theoretical analysis. Like the alternative transform methods, it is a mathematically reversible function, thereby allowing for signal reconstruction, possibly after removal of specific components.

CEEMD performs exceptionally well overcoming mode-mixing problems. The reconstruction error is around machine precision (Torres et al., 2011). The computation of the instantaneous frequency from the isolated modes leads to a well-defined time-frequency representation. SST shares many of the advantages of CEEMD in practice, with an acceptable reconstruction error. Thus, both methods are suitable to decompose a seismic trace into individual components with the advantage of frequency localization. It may also aid in noise-attenuation problems in which the signal and noise correspond to different components, likewise, a recently proposed technique based on regularized nonstationary autoregression (Fomel, 2013). As in this paper, Fomel (2013) also suggests seismic data compression and seismic data regularization as possible applications for seismic data decomposition into spectral components. Both approaches aim to decompose seismic data into a sum of oscillatory signals with smoothly varying frequencies and smoothly varying amplitudes (Fomel, 2013; Thakur et al., 2013), which is the principle of the decomposition using the CWT (Daubechies et al., 2011).

CEEMD using 50 noise realizations is approximately 13 times slower than SST using our parameter settings; SST has approximately the same cost as a WT, yet neither method is prohibitively expensive. We found that by using a classical Morlet wavelet and 32 levels for the SST method, we get a good balance between speed and resolution in the frequency representation. The improvement of SST is clear compared with the CWT. The reassignment technique plays an important role in the results, by reallocating the wavelet energy to the corresponding time position.

CEEMD and SST are more appropriate than STFT and CWT when better time-frequency localization is needed. On the other hand, STFT and CWT remain very useful analysis methods, even if they may be subject to more spectral leakage than the CEEMD and SST methods, because they do not collapse spectra to narrow frequency bands. For instance, many attenuation methods are based on spectral ratios between two signals (Reine et al., 2009, 2012). Spectral ratios are difficult to compute if only individual frequency lines exist. On the other hand, it may be possible to use the frequency-shift method (Quan and Harris, 1997) to estimate seismic attenuation using the CEEMD and SST methods. SST, due to the reassignment step, will concentrate the energy into a small spectral band. Thus, it will be more appropriate when better time-frequency localization is needed (such as stratigraphic mapping to detect channel structures or identification of resonance frequencies).

From our study, we find that SST and CEEMD perform equally well for seismic time-frequency representation, with the advantage of speed and a stronger mathematical foundation in the case of the SST. A further difference is that in the SST method, one can specify the frequency range of interest prior to decomposition via the CWT scale parametrization. This can speed up computations in many
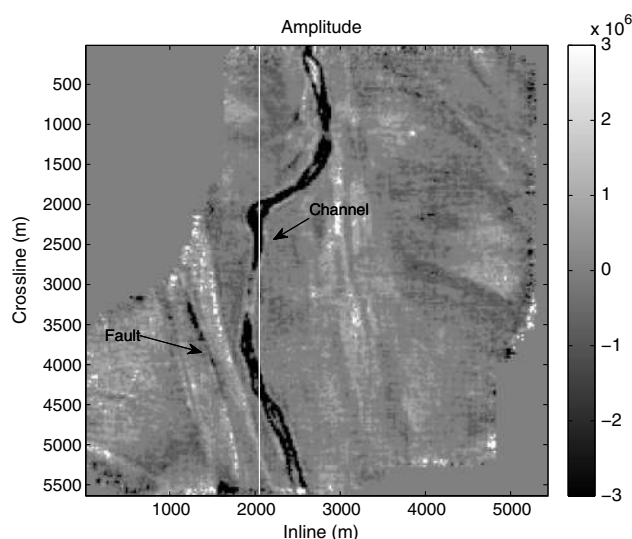

Figure 10. Time slice at 420 ms. The channel and fault are clearly visible. The vertical white line, at inline 2050 m, represents the section displayed in Figure 6.
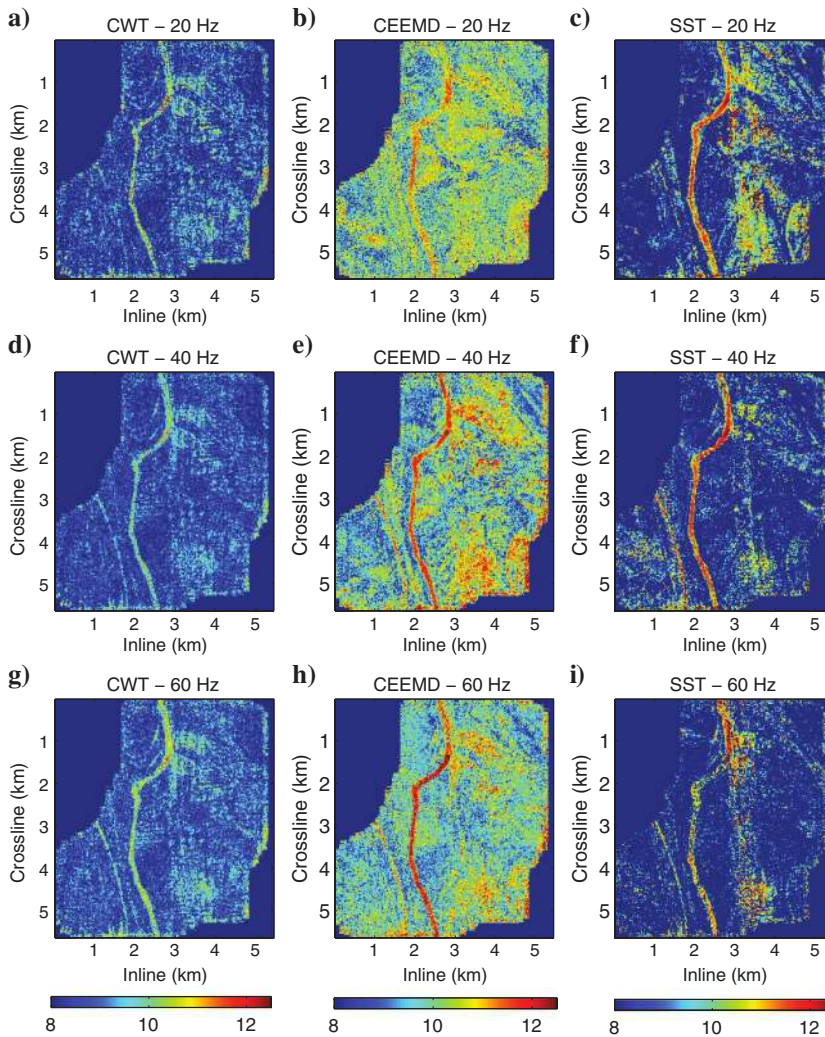
Figure 11. Constant-frequency slices. (a) Shows from top to bottom the CWT outputs for 20, 40, and 60 Hz, respectively. (b) The corresponding instantaneous spectrum estimated by CEEMD. The SST output is shown in (c).

situations, whereas in CEEMD, components are always estimated sequentially starting with the highest frequency ones.

CONCLUSIONS

The SST has a strong mathematical foundation based on frequency reassignment of WT decompositions. In simple applications, SST and CEEMD give comparable results, although in more complex situations, SST can yield more favorable results because it has the ability to adapt the mother wavelet to the data under consideration. On the other hand, the advantage of CEEMD and variants is precisely the fact that no decomposition basis needs to be specified, eliminating the possible requirement to test for performance enhancements by changing the decomposition basis.

SST produces an acceptable reconstruction error, which improves as we extend the level of decomposition. This frequency-based decomposition method can reconstruct individual components from selected frequency bands. SST is therefore attractive for high-resolution time-frequency analysis of seismic signals.

REFERENCES

Auger, F., and P. Flandrin, 1995, Improving the readability of time-frequency and time-scale representations by the reassignment method: IEEE Transactions on Signal Processing, **43**, 1068–1089, doi: 10.1109/78.382394.

Barnes, A. E., 1993, Instantaneous spectral bandwidth and dominant frequency with applications to seismic reflection data: Geophysics, **58**, 419–428, doi: 10.1190/1.1443425.

Daubechies, I., 1992, Ten lectures on wavelets: SIAM, CBMS-NSF Regional Conference Series in Applied Mathematics.

Daubechies, I., J. Lu, and H.-T. Wu, 2011, Synchrosqueezed wavelet transforms: An empirical mode decomposition-like tool: Applied and Computational Harmonic Analysis, **30**, 243–261, doi: 10.1016/j.acha.2010.08.002.

Daubechies, I., and S. Maes, 1996, A nonlinear squeezing of the continuous wavelet transform based on auditory nerve models, in A. Aldroubi, and M. Unser, eds., Wavelets in medicine and biology: CRC Press, 527–546.

Donoho, D., 1995, De-noising by soft-thresholding: IEEE Transactions on Information Theory, **41**, 613–627, doi: 10.1109/18.382009.

Fomel, S., 2013, Seismic data decomposition into spectral components using regularized nonstationary autoregression: Geophysics, **78**, no. 6, O69–O76, doi: 10.1190/geo2013-0221.1.

Hall, M., 2006, Resolution and uncertainty in spectral decomposition: First Break, **24**, 43–47.

Han, J., R. H. Herrera, and M. Van der Baan, 2013, Spectral decomposition by synchrosqueezing transform: Presented at 75th EAGE Conference and Exhibition.

Han, J., and M. Van der Baan, 2013, Empirical mode decomposition for seismic time-frequency analysis: Geophysics, **78**, no. 2, O9–O19, doi: 10.1190/geo2012-0199.1.

Herrera, R. H., R. Orozco, and M. Rodriguez, 2006, Wavelet-based deconvolution of ultrasonic signals in nondestructive evaluation: Journal of Zhejiang University SCIENCE A, **7**, 1748–1756, doi: 10.1631/jzus.2006.A1748.

Huang, N. E., Z. Shen, and S. R. Long, 1999, A new view of nonlinear water waves: The Hilbert spectrum: Annual Review of Fluid Mechanics, **31**, 417–457, doi: 10.1146/annurev.fluid.31.1.417.

Huang, N. E., Z. Shen, S. R. Long, M. C. Wu, H. H. Shih, Q. Zheng, N.-C. Yen, C. C. Tung, and H. H. Liu, 1998, The empirical mode decomposition and the Hilbert spectrum for nonlinear and non-stationary time series analysis: Proceedings of the Royal Society of London, Series A: Mathematical, Physical and Engineering Sciences, **454**, 903–995, doi: 10.1098/rspa.1998.0193.

Huang, N. E., M.-L. C. Wu, S. R. Long, S. S. Shen, W. Qu, P. Gloersen, and K. L. Fan, 2003, A confidence limit for the empirical mode decomposition and Hilbert spectral analysis: Proceedings of the Royal Society of London, Series A: Mathematical, Physical and Engineering Sciences, **459**, 2317–2345, doi: 10.1098/rspa.2003.1123.

Li, C., and M. Liang, 2012, A generalized synchrosqueezing transform for enhancing signal time-frequency representation: Signal Processing, **92**, 2264–2274, doi: 10.1016/j.sigpro.2012.02.019.

Mallat, S., 2008, A wavelet tour of signal processing: The sparse way, 3rd ed.: Academic Press.

Meignen, S., T. Oberlin, and S. McLaughlin, 2012, A new algorithm for multicomponent signals analysis based on synchrosqueezing: With an application to signal sampling and denoising: IEEE Transactions on Signal Processing, **60**, 5787–5798, doi: 10.1109/TSP.2012.2212891.

Partyka, G., J. Gridley, and J. Lopez, 1999, Interpretational applications of spectral decomposition in reservoir characterization: The Leading Edge, **18**, 353–360, doi: 10.1190/1.1438295.

Perz, M., 2001, Coals and their confounding effects: CSEG Recorder, **26**, no. 12, 34–53.

Quan, Y., and J. M. Harris, 1997, Seismic attenuation tomography using the frequency shift method: Geophysics, **62**, 895–905, doi: 10.1190/1.1444197.

Reine, C., R. Clark, and M. van der Baan, 2012, Robust prestack Q-determination using surface seismic data: Part 1 — Method and synthetic examples: Geophysics, **77**, no. 1, R45–R56, doi: 10.1190/geo2011-0073.1.

Reine, C., M. Van der Baan, and R. Clark, 2009, The robustness of seismic attenuation measurements using fixed- and variable-window time-frequency transforms: Geophysics, **74**, no. 2, WA123–WA135, doi: 10.1190/1.3043726.

Thakur, G., E. Brevdo, N. S. Fučkar, and H.-T. Wu, 2013, The synchrosqueezing algorithm for time-varying spectral analysis: Robustness properties and new paleoclimate applications: Signal Processing, **93**, 1079–1094, doi: 10.1016/j.sigpro.2012.11.029.

Torres, M., M. Colominas, G. Schlotthauer, and P. Flandrin, 2011, A complete ensemble empirical mode decomposition with adaptive noise: IEEE International Conference on Acoustics, Speech and Signal Processing (ICASSP), 4144–4147, doi: 10.1109/ICASSP.2011.5947265.

Van der Baan, M., S. Fomel, and M. Perz, 2010, Nonstationary phase estimation: A tool for seismic interpretation?: The Leading Edge, **29**, 1020–1026, doi: 10.1190/1.3485762.

Wu, H.-T., P. Flandrin, and I. Daubechies, 2011, One or two frequencies? The synchrosqueezing answers: Advances in Adaptive Data Analysis, **3**, no. 2, 29–39, doi: 10.1142/S179353691100074X.

Wu, Z., and N. E. Huang, 2009, Ensemble empirical mode decomposition: A noise-assisted data analysis method: Advances in Adaptive Data Analysis, **1**, no. 1, 1–41, doi: 10.1142/S1793536909000047.